# Instantaneous and time-averaged flow structures around a blunt double-cone with or without supersonic film cooling visualized via nano-tracer planar laser scattering*

Zhu Yang-Zhu(朱杨柱), Yi Shi-He(易仕和)†, He Lin(何 霖), Tian Li-Feng(田立丰), and Zhou Yong-Wei(周勇为)

*College of Aerospace Science and Engineering, National University of Defense Technology, Changsha* 410073, *China*

(Received 30 April 2012; revised manuscript received 5 September 2012)

In a Mach 3.8 wind tunnel, both instantaneous and time-averaged flow structures of different scales around a blunt double-cone with or without supersonic film cooling were visualized via nano-tracer planar laser scattering (NPLS), which has a high spatiotemporal resolution. Three experimental cases with different injection mass flux rates were carried out. Many typical flow structures were clearly shown, such as shock waves, expansion fans, shear layers, mixing layers, and turbulent boundary layers. The analysis of two NPLS images with an interval of 5 μs revealed the temporal evolution characteristics of flow structures. With matched pressures, the laminar length of the mixing layer was longer than that in the case with a larger mass flux rate, but the full covered region was shorter. Structures like K–H (Kelvin–Helmholtz) vortices were clearly seen in both flows. Without injection, the flow was similar to the supersonic flow over a backward-facing step, and the structures were relatively simpler, and there was a longer laminar region. Large scale structures such as hairpin vortices were visualized. In addition, the results were compared in part with the schlieren images captured by others under similar conditions.

**Keywords:** blunt cone, supersonic flow structure, flow visualization, supersonic film cooling

**PACS:** 47.40.Ki, 47.80.Jk, 47.40.–x, 47.80.–v **DOI:** 10.1088/1674-1056/22/1/014702

## 1. Introduction

During supersonic or hypersonic travel, the flight vehicle surface is surrounded by a high-temperature environment after a bow shock wave, thus the surface material requires more rigidity and intensity.[1] So the vehicle surface must be cooled. Instead of using special materials, supersonic film cooling is widely used as an economic way to protect the vehicle wall from the high-temperature air.[2] It is a thin layer or film of relatively low temperature gas injected parallel to the wall surface. However, the flow field with injection is more complex for many added structures involving mixing layers, shocks, turbulent boundary layers, etc. Based on Seban's research,[3] the film cooling flow field can be divided into three regions: an inviscid core region, a wall jet region, and a boundary layer region. The inviscid core region, like a free jet, contains a viscous layer that emanates from the lip and ends when it meets the growing slot flow boundary layer. In this region, the wall temperature remains a constant at the recovery value of the injection. The wall jet region starts at the location where the viscous layer originating from the lip meets the slot flow boundary layer. In this region, the wall begins to be affected by the mixing between the mainstream and the injection. Due to the intense mixing in this region, the temperature starts to approach that of the mainstream value. Further downstream, the wall injection relaxes to a boundary layer flow. In order to further investigate the characteristics of the flow field around the vehicle surface with or without film cooling, it is important to observe the fine structures of a flow.

In the past decades, to the authors' knowledge, visualizations of supersonic flow fields were mostly obtained utilizing schlieren photography or shadowgraphy.[4–6] In the investigation carried out by Juhany *et al.*,[7] a schlieren photograph of Mach number 2.2 air injection with Mach number 2.4 mainstream was captured. The injection and the mainstream were matched at pressure. In their study, the shock and the expansion waves were visible, but the structures inside the boundary layer and the interaction were not clearly given. Using shadowgraphy, Mark and Roy[6] have investigated the two-dimensional flow field of slot injection into a supersonic flow with an adverse pressure gradient. The Mach 2 supersonic tunnel was operated at a total pressure of 400 kPa, and three shock train locations corresponding to back pressures of 125 kPa, 200 kPa, and 225 kPa were evaluated. The results showed that by increasing the injection total pressure, the under-expanded jet increases in length and thickness, resulting in increases in the incidence angle and the strength of the jet-induced shock. Some other relevant studies in this field are ongoing.[8–17]

Due to the low spatial resolution and the integral effect of the two methods above, they are not very suitable for revealing fine structures in a complicated supersonic flow. In addition, planar laser induced fluorescence (PLIF)[18] and filtered

*Project supported by the National Basic Research Program of China (Grant No. 2009 CB724100) and the National Natural Science Foundation of China (Grant No. 11172326).

†Corresponding author. E-mail: ysh_1819@yahoo.com.cn

© 2013 Chinese Physical Society and IOP Publishing Ltd 

Rayleigh scattering (FRS),[19,20] which have been used widely in recent years, are also inadequate considering the low scattering signal, low signal-to-noise ratio (SNR), and high cost.

Nano-tracer planar laser scattering (NPLS) is a new flow visualization technique for measuring the fine structures of a supersonic/hypersonic flow. It has a spatial resolution up to the micron scale and a time resolution up to 6 ns. Gao *et al.* have investigated the aero-optical effects caused by a supersonic mixing layer via NPLS.[21] In this experimental work, the NPLS technique is used to study the supersonic flow field around a blunt double-cone[22] with or without supersonic film coolings of different injection mass flux rates.

## 2. Experimental setup

### 2.1. Supersonic wind tunnel and testing model

As shown in Fig. 1, the experimental study is carried out in a low noise supersonic indraft wind tunnel with dry air as the working gas. The stabilization chamber is a square channel long enough connected via a short transitional section with a round valve which is used to control the air inlet. The nozzle of the wind tunnel can be replaced, and the one used in this experiment is of Mach 3.8. The cross section of the testing chamber is a 100 mm×120 mm rectangle, and the dimensions of its three side faces encased with high quality optical glass convenient for light transfer are 250 mm×100 mm and 250 mm×120 mm. Key parameters of the wind tunnel running are listed in Table 1.



**Fig. 1.** The supersonic wind tunnel.

**Table 1.** Key parameters of wind tunnel, where $M_\infty$, $P_0$, $\rho_\infty$, $T_0$, $T_\infty$, $Re_\infty$, and $U_\infty$ are Mach number, stagnation pressure, density, stagnation temperature, static pressure, Reynolds number, and velocity of the free stream, respectively.

| $M_\infty$ | $P_0$/MPa | $\rho_\infty$/kg·m$^{-3}$ | $T_0$/K | $T_\infty$/K | $Re_\infty$/m$^{-1}$ | $U_\infty$/m·s$^{-1}$ |
|---|---|---|---|---|---|---|
| 3.8 | 0.1 | 0.039 | 300 | 77 | $6.5\times10^6$ | 669 |

The test model is shown in Fig. 2, which is a three-dimensional blunt double-cone with an injector nozzle in the forehead. Designed based on a *B*-spline curve, the injector nozzle whose slot exit height is 3 mm can supply a homogeneous and stable supersonic flow of Mach 2.5 to cover the model wall, with air as the injectant supplied by the gas of the wind tunnel stabilization chamber. The lip whose thickness is only 0.2 mm has a wedge shape with a sharp trailing edge. A small stabilization chamber is set inside the model to stabilize the inflow air. The injection mass flux rate can be adjusted by a stagnation pressure regulator fixed upstream to match the pressures of the film and the mainstream after the head bow shock. In this paper, three experimental cases are carried out as listed in Table 2.

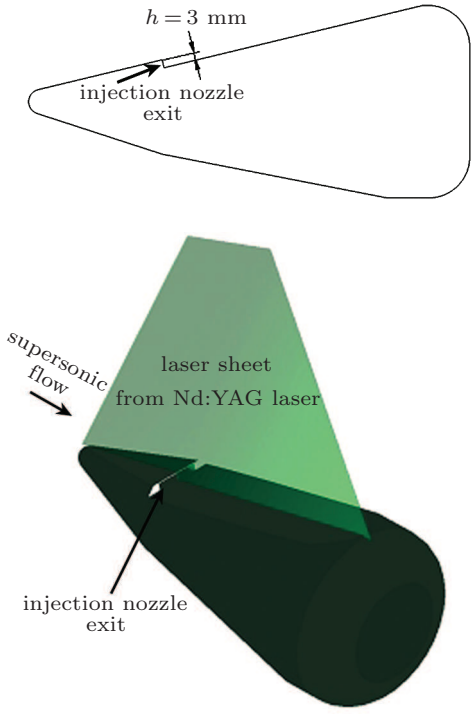



**Fig. 2.** (color online) Schematic diagram of testing model.

**Table 2.** Primary parameters of injection working cases, where $h$ is the slot exit height; $M_\mathrm{i}$, $\dot{m}$, $P_{0\mathrm{i}}$, $P_\mathrm{i}$, $T_\mathrm{i}$, $\rho_\mathrm{i}$, $U_\mathrm{i}$, and $Re_\mathrm{i}$ are Mach number, mass flux rate, stagnation pressure, static pressure, static temperature, density, velocity, and Reynolds number of the injection, respectively; and $\rho_\mathrm{m}$ and $U_\mathrm{m}$ are density and velocity of the mainstream, respectively.

| Case | $h$/mm | $M_\mathrm{i}$ | $\dot{m}$/g·s$^{-1}$ | $P_{0\mathrm{i}}$/MPa | $P_\mathrm{i}$/Pa | $T_\mathrm{i}$/K | $\rho_\mathrm{i}$/kg·m$^{-3}$ | $U_\mathrm{i}$/m·s$^{-1}$ | $Re_\mathrm{i}$/$10^6$ m$^{-1}$ | $\rho_\mathrm{m}$/kg·m$^{-3}$ | $U_\mathrm{m}$/m·s$^{-1}$ |
|---|---|---|---|---|---|---|---|---|---|---|---|
| I | 3 | 2.5 | 0.24 | 0.05 | 2926 | 135 | 0.075 | 578 | 5.6 | 0.08 | 660 |
| II | 3 | 0 | – | – | – | – | – | – | – | – | – |
| III | 3 | 2.5 | 0.48 | 0.1 | 5853 | 135 | 0.15 | 578 | 11.3 | 0.08 | 660 |

### 2.2. NPLS technique

The NPLS is a new technique for flow visualization, which was developed recently by a research group at the National University of Defense Technology. Nanoparticles have good flow-following ability, and can follow flow fluctuations in supersonic flows,[23] which have been adopted as tracers in the NPLS technique. Supersonic flow structures such as shock waves, turbulent boundary layers, mixing layers, Mach disks, and sliding lines have been visualized in previous experiments

using this technique.[23–29]

As shown in Fig. 3, an NPLS system consists of a computer, an interline transfer double-exposure CCD camera, a nanoparticle generator, a synchronizer, and a $Q$-switched frequency-doubled (dual-cavity) Nd:YAG laser. The flow seeded by the titanium dioxide ($TiO_2$) particles with a nominal median diameter of 50 nm is illuminated by the laser with 500 mJ pulsed energy and 6 ns pulse duration at the wavelength of 532 nm. The direction of the laser is adjusted by using a beam oriented arm, and the laser sheet formed through the lens group is approximately 0.5 mm thick. The sensor of the CCD has 2K×2K pixels, and the step gray scale is up to 4096. Two frames of a supersonic flow can be recorded via frame-straddling[30] within a double-exposure interval, which can be as short as 200 ns.

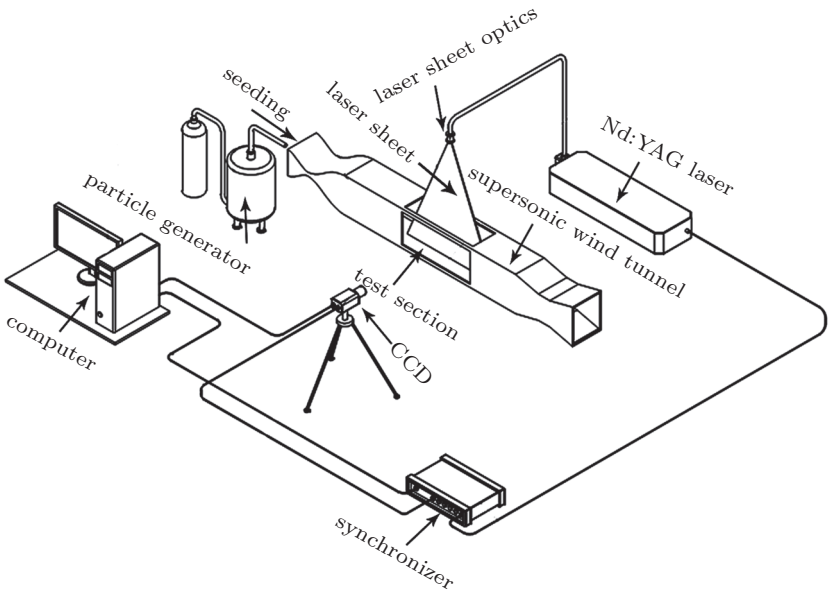



**Fig. 3.** Schematic diagram of the NPLS system.[31]

## 3. Fine flow structure visualization and discussion

As listed in Table 2, three experimental cases were carried out respectively. In case I, the pressures of the injection slot exit and the mainstream above matched. In case II, there was no injection. In case III, the pressure of the injection slot exit was larger than that of the mainstream above. Fine images of the flows in the symmetric plane of the model with high spatio-temporal resolution were obtained via the NPLS technique. Time-averaged flow characteristics will be discussed based on a large number of NPLS images. The result from test case I will be discussed first as it best demonstrates the key features of a supersonic film cooling flow.

### 3.1. Flow visualization for case I

The instantaneous NPLS images from case I are shown in Figs. 4(a) and 4(b). In this case, the pressure of the injection slot exit is 2926 Pa, which matches the pressure of the mainstream above. The spatial resolution of the NPLS image is 94 μm/pixel, and the interval between Fig. 4(a) and Fig. 4(b) is 5 μs. The flow field region is 192 mm×91 mm.

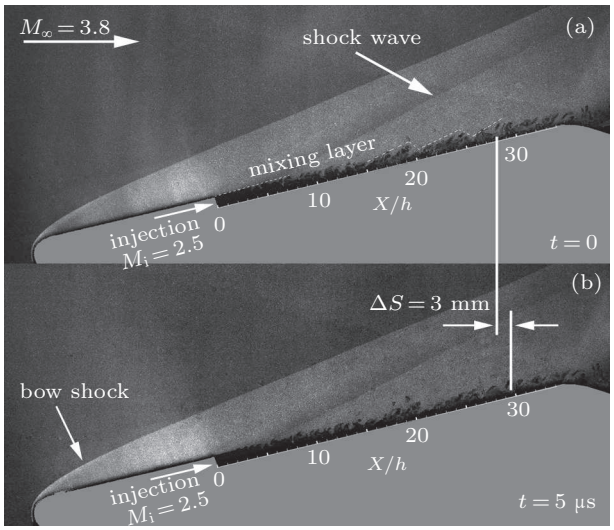



**Fig. 4.** NPLS images at (a) $t = 0$ μs and (b) $t = 5$ μs of case I.

Fine structures are revealed in NPLS images. In a flow of Mach 3.8, a bow shock appears around the head of the double-cone. Because of the good flow-following ability of nanoparticles, the shock is very thin. And after the shock, the gray increases rapidly in result of the density increasing compared

to the front.[32] A laminar boundary layer forms on the head of the model, and its mean thickness is about $0.2h$. In this case, the injection and the mainstream pressures are matched, but a shock wave reflected by the model wall forms at about $X = 5h$ downstream from the lip with an angle of 13.9° relative to the wall. The shock wave is also seen in the schlieren image shown in Fig. 5 which was captured by Maqbool.[33] Contrasting to the NPLS image, the resolution of the schlieren image is lower, and the shock wave is thicker. In the NPLS images, it is shown that the interaction between the injection and the mainstream starts from the slot lip, and a supersonic-to-supersonic mixing layer is clearly presented. It is found that a laminar shear layer acts in the area of $X$=0–$2.5h$, and from about $X$=$2.5h$, the mixing layer is destabilized, K–H (Kelvin–Helmholtz) vortexes appear and develop downstream. Further downstream, the vortexes grow larger until breaking. After then, the two flows mix completely and turn to a turbulent boundary layer above the wall. The upper growth rate of the mixing layer is 0.034, while the lower one is −0.087. Measured in the NPLS image, the film protection length is about $15h$, during which the wall can be protected best, and after the point the turbulent boundary layer develops with the intermittency phenomenon and is clearly seen. Large-scale structures can be measured accurately in NPLS images, which are difficult to obtain by using schlieren photography. During the 5 μs interval of the two NPLS images, a vortex, which is marked by the vertical lines, moves 3 mm horizontally, while its shape changes little. This proves that the turbulent structure has characteristics of being quick moving but having slow deformation.



**Fig. 5.** (color online) Schlieren image with injection captured by Maqbool *et al.*[33]

Mach numbers of the mainstream and the injection are 2.26 and 1.2, respectively, and the two flow pressures are matched. Velocity and density ratio of injection to mainstream are 1.30 and 0.57, respectively.

A time-averaged flow field based on NPLS images by repeating measurements can be obtained as shown in Fig. 6. Though some transient characters are blotted out in the averaging process, some flow unsteadiness is also eliminated, which is convenient for acquiring and analyzing the time-averaged structural features. It can be seen that the laminar boundary layer above the head of the model is very thin (about $0.2h$), and due to the lip disturbance, a weak Mach wave which is 20.4° initially and 15.5° lastly relative to the model wall is visible, but not obviously in the instantaneous image. The upper growth angle of the mixing layer relative to the wall is 1.83°. The reflected shock wave is 13.9° relative to the wall. Fine structures are blurred, but the edge of the turbulent layer can be measured, and the edge is approximately parallel to the wall.

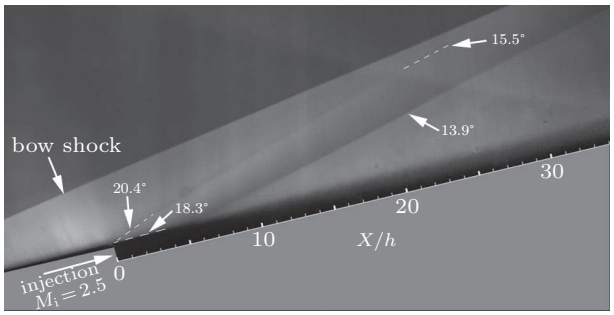



**Fig. 6.** Time-averaged flow field of case I.

### 3.2. Flow visualization for case II

An instantaneous NPLS image for case II is shown in Fig. 7. The resolution of the NPLS image is 94 μm/pixel, and the flow region is 153 mm×63 mm. When there is no injection, the flow characteristics are much different compared to those in case I, but similar to those in the backward facing step (BFS) flow.[31,34] In the same way, a bow shock wave forms around the model head under the action of Mach 3.8 flow, but in much different way; an expansion fan is visible, which is produced when the supersonic flow after the bow shock expands around the backward facing step. After passing over the step, the flow accelerates with the direction changing and density decreasing, corresponding to the dark region of the NPLS image. As shown in Fig. 7, the recirculation region at the corner of the step is from the lip to about $6h$ downstream, and a free shear layer is formed with the mainstream between the separated flow and the recirculation region. The heat flux to the model surface in the recirculation region will be small, but it will rise sharply after the reattachment point.[33] The reattachment occurs at the point of $X = 6h$, where a shock is produced by the converging compressible waves when the flow meets the wall. The angle of this shock (termed the reattachment shock) relative to the upper surface plane of the model is 12.8°. A new boundary layer develops further after the reattachment, whose thickness increases from 1.05 mm at $X = 10h$ to 4.92 mm at $X = 30h$. In the region of $X = 6$–$15h$, some quasi-ordering structures appear and grow gently. Over $X = 18h$, the boundary layer transits to a developed turbulence. Fine structures such as hairpin vortices in the boundary layer can be observed distinctly. A schlieren image has been obtained by Maqbool *et al.*,[33] as shown in Fig. 8. A similar wave system is shown, but the fine structures in the boundary layer cannot be measured accurately.

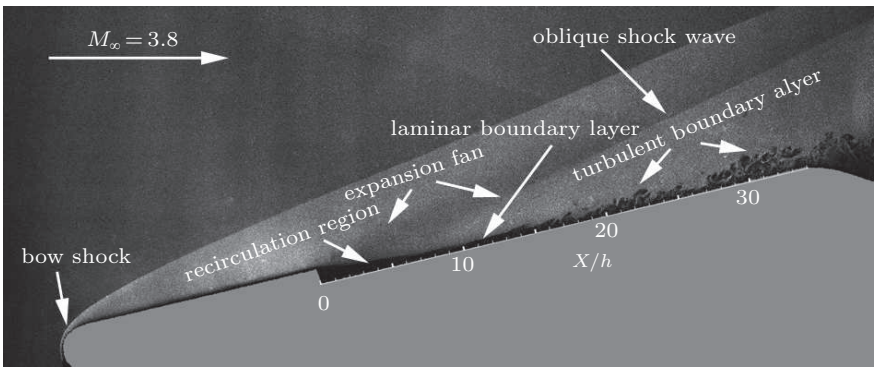



**Fig. 7.** NPLS image of case II.



**Fig. 8.** (color online) Schlieren image without injection captured by Maqbool *et al.*[33]

Figure 9 shows a time-averaged result based on a large number of NPLS images in case II. As a result of the disturbance of the backward facing step, the flow over it expands with density decreasing so that the expansion fan region is dark with an angle of 20.3°. The reattachment shock is 12.8° relative to the wall, 7.9% smaller than the angle of the reflected shock in case I. After the reattachment point, the supersonic boundary layer thickness increases at an angle of 2.4°.

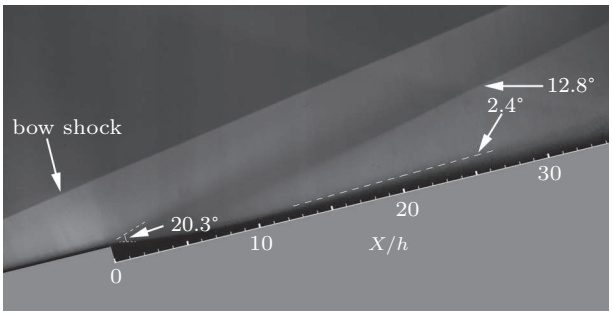



**Fig. 9.** Time-averaged flow field of case II.

### 3.3. Flow visualization for case III

The fine structure visualization for case III is shown in Fig. 10. The resolution of the NPLS image is 94 μm/pixel, and the flow region is 153 mm×65 mm. In this case, the injection static pressure is 5853 Pa, which is larger than that of the mainstream, and the mass flux rate is 0.48 g/s, which is two times of that in case I.

Besides the same bow shock in Mach 3.8, there is a shock near the slot lip whose angle is 21.9° relative to the wall. It is induced due to the higher pressure of the injection. A shock reflected by the wall in the injection also emerges but with a larger mass flux rate of the injection, the shock foot moves downstream to $X = 10h$. The shock angle relative to the wall is 13.7°. The mixing layer between the injection and the mainstream uptilts a little because of the larger mass flux rate. The full protection length of the model wall is about $18h$, which is longer than that in case I. According to the work of Pedersen,[35] a higher density ratio of this case can improve the cooling effectiveness. The laminar length of the mixing layer is about $4h$, and the turbulent region is larger.

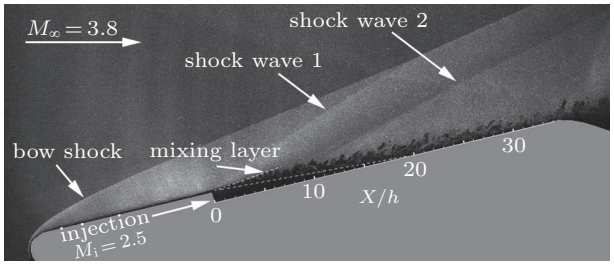



**Fig. 10.** NPLS image of case III.

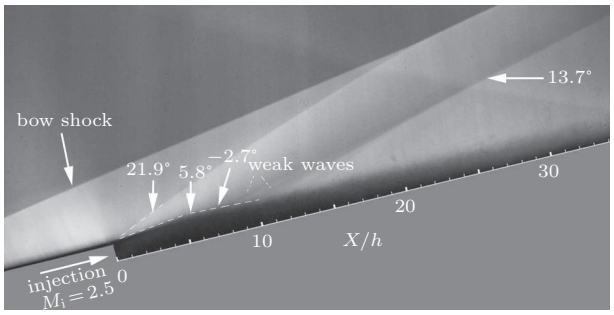



**Fig. 11.** Time-averaged flow field of case III.

The time-averaged image based on NPLS images is shown in Fig. 11. After a bow shock, the scattering light becomes stronger corresponding to the density increasing rapidly, so the region becomes brighter. The shock due to the higher slot exit pressure is at an angle of 21.9°, while the lip Mach wave angle is 20.4°. The mixing layer upper edge angle is about 5.8° for about $5h$ duration, and then it changes to −2.7°. In the adjacent region of $X$=10$h$, there are some weak

waves. The reflected shock angle is 13.7°, which is not very different from that in case I.

### 3.4. Comparing and discussion

Contrasting to that in case I, the transition of the mixing layer in case III is earlier. Without the injection, the boundary layer will cover almost all the wall except for a short recirculation region. In this case, the model wall cannot be protected from the high temperature environment. When the injection works, the flow field becomes more complex, because the injection mixes with the mainstream and many waves and vortices come out. As shown in the NPLS images above, the wall can be protected by the injection to a certain extent, and improving the injectant mass flux rate will make the protected length increase. In cases I and III, K–H vortices in the mixing layer are both observed. During the first short distance, the vortices are perpendicular to the injection flow and the mainstream on the whole, as the velocity difference of the two flows is not remarkable. However, after that, due to the exchange of energy and momentum among injection, mainstream, and boundary layer above the model surface, the vortices start to incline to the wall gradually. The interaction between injection and mainstream in case III is relatively stronger for the double mass flux rate. Moreover, more shock waves and a thicker boundary layer emerge. The shocks shown in time-averaged NPLS images are clearly seen with sharp edges without the integral effects of schlieren. It suggests that the position of shocks is approximately stable under the condition of the same basic flow parameters though the different scale structures are varying. The angles of the reflected shock in cases I and III are not affected by the different mass flux rates markedly.

## 4. Conclusion

Fine structures of flow around a blunt double-cone with supersonic film cooling in three different mass flux regimes were investigated via the NPLS technique in this paper. The representative structures such as shocks, expansion fans, laminar boundary layer, turbulent boundary layer, and mixing layer were revealed clearly. The results indicated that NPLS images have advantages of high spatial resolution to micron scale and good temporal resolution to nanosecond scale. Unlike schlieren photography and shadowgraphy, the NPLS image can reveal the fine structures in boundary and mixing layers, and at the same time, the shock is very thin as a result of the fine flow-following ability of the nanoparticles. The K–H and the hairpin vortices are clearly visible in NPLS images. Without injection, the flow structures are relatively simpler, and there is a longer laminar region after the reattachment besides that the turbulent boundary layer acts downstream above the model wall. Characteristics of time-average flow fields were investigated based on many NPLS images in the same experimental case. It was found that the turbulent boundary layer growth angle after the reattachment is about 2.4° if no injection works. With matched pressures, the mixing and the turbulent layers are approximately parallel to the wall. However, with a double mass flux rate of the injection , there is a turning point at about $X = 5h$, and after the mixing action, the boundary layer is still parallel to the wall.

## References


[1] Li G C 2006 *Aero-optics* (Beijing: National Defense Industry Press) pp. 12–17 (in Chinese)
[2] Eckert E R G 1952 *Heat-Transfer Symposium,* Michigan, American p. 195
[3] Seban R A and Back L H 1962 *Journal of Heat Transfer* **84** 45
[4] Daanish M, Krian D and Christopher C 2010 *AIAA Paper* 2010-6886
[5] Aupoix B, Mignosi A, Viala S, Bouvier F and Gaillard R 1998 *AIAA Paper* 96-0657
[6] Mark A and Roy J 1993 *AIAA Paper* 93-2442
[7] Juhany K A, Hunt M L and Sivo J M 1994 *Journal of Thermophysics and Heat Transfer* 8 59
[8] Singh M, Singh L P and Husain A 2011 *Chin. Phys. Lett.* **28** 094701
[9] Singh L P, Husain A and Singh M 2010 *Chin. Phys. Lett.* **27** 014702
[10] Wang L and Lu X Y 2011 *Chin. Phys. Lett.* **28** 064702
[11] Cao Y H, Pei J, Chen J and She Z S 2008 *Chin. Phys. Lett.* **25** 3315
[12] Xu J L and Ma H Y 2007 *Chin. Phys. Lett.* **24** 763
[13] Lian Q X and Guo H 2004 *Acta Phys. Sin.* **53** 2226 (in Chinese)
[14] Zhao D M and Zhang Q C 2010 *Chin. Phys.* B **19** 030518
[15] Liu S L, Zhang L M, Chen C X, Ma X X and Zhu N L 1995 *Acta Phys. Sin.* B **44** 825
[16] Li S H, Liu B C, Ni G Q and Xu Z Z 2003 *Chin. Phys.* B **12** 0856
[17] Jiang S E, Yang J M, Zheng Z J and Ding Y K 2007 *Chin. Phys.* B **16** 0193
[18] Meyer T R 2002 *Exp. in Fluids* **32** 603
[19] Elliott G S, Glumac N and Carter C D 1999 *AIAA Paper* 99-0643
[20] Fu P T, Han J F, Mou Y H, Han D and Yang C W 2011 *Acta Phys. Sin.* **60** 053602 (in Chinese)
[21] Gao Q, Yi S H, Jiang Z F, Zhao Y X and Xie W K 2012 *Chin. Phys.* B **21** 064701
[22] Han J and Jiang N 2008 *Chin. Phys. Lett.* **25** 1731
[23] Zhao Y X, Yi S H, Tian L F and Cheng Z Y 2009 *Sci. China Ser.* E **52** 3640
[24] Zhao Y X, Yi S H, He L, Cheng Z Y and Tian L F 2007 *Chin. Sci. Bull.* **52** 1297
[25] Zhao Y X, Yi S H, He L, Cheng Z Y and Tian L F 2007 *Journal of National University of Defense Technology* **29** 12 (in Chinese)
[26] Zhao Y X, Yi S H, Tian L F, He L and Cheng Z Y 2008 *Sci. China Ser.* G **51** 1134
[27] Yi S H, He L, Zhao Y X, Tian L F and Cheng Z Y 2009 *Sci. China Ser.* G **52** 2001
[28] He L, Yi S H, Zhao Y X, Tian L F and Chen Z 2011 *Chin. Sci. Bull.* **56** 489
[29] Yang W B, Zhuang F G, Shen Q, Guan F M, Wang Q, Yi S H, Zhao Y X, He L and Tian L F 2009 *Sci. China Ser.* G **52** 1624
[30] Hornak J P 2002 *Encyclopedia of Imaging Science and Technology* (New York: John Wiley and Sons) p. 390
[31] Chen Z, Yi S H, Tian L F, He L and Zhu Y Z 2012 *Shock Waves* (published online)
[32] Tian L F, Yi S H, Zhao Y X, He L and Cheng Z Y 2009 *Sci. China Ser.* G **52** 1357
[33] Maqbool D 2010 *Development of an Experiment for Measuring Film Cooling Performance in Supersonic Flows* (M. S. thesis) (College Park: the University of Maryland)
[34] Chen Z, Yi S H and He L 2012 *Chin. Sci. Bull.* **57** 584
[35] Pedersen D, Eckert E and Goldstein R 1977 *Journal of Heat Transfer* **99** 620